Flexible Asymmetric Supercapacitor Based on Structure-Optimized Mn_3O_4/Reduced Graphene Oxide Nanohybrid Paper with High Energy and Power Density

*Yating Hu, Cao Guan, Guangxue Feng, Qingqing Ke, Xiaolei Huang, and John Wang**

A highly flexible Mn_3O_4/reduced graphene oxide (rGO) nanohybrid paper with high electrical conductivity and high mass loading of Mn_3O_4 nanofibers (0.71 g cm^{-3}) is developed via a facile gel formation and electrochemical reduction process, which is low-cost, environmental friendly, and easy to scale up. Confined Mn_3O_4 nanofibers are well dispersed within the rGO sheets, which demonstrate to be a promising cathode material for flexible asymmetric supercapacitors (ASCs). When coupled with an electrochemically reduced rGO paper as the anode, a flexible ASC device, based on the Mn_3O_4/rGO nanohybrid paper as the cathode, is assembled; and it demonstrates remarkable electrochemical performance: a high volumetric capacitance of 54.6 F cm^{-3} (546.05 mF cm^{-2}), and remarkable volumetric energy and power density (0.0055 Wh cm^{-3} and 10.95 W cm^{-3}) being achieved with excellent cycling ability. The nanohybrid paper shows great improvement for flexible energy devices in terms of electrochemical properties.

1. Introduction

Flexible energy storage devices are drawing considerable attention of research and development due to the rapidly growing demand in flexible, portable, and wearable electronic devices as well as for electric and hybrid vehicles.[1] Flexible supercapacitors require the electrode material to have the desired electrochemical functions with well-integrated mechanical flexibility,[2] thus typical flexible supercapacitors are based on highly flexible thin-film electrode with soft materials as substates.[3] Among the candidates for thin-film electrodes, carbon-based materials (e.g., graphene, carbon nanotube (CNT), carbon cloth, etc.) possess the high mechanical strength to withstand bending, folding or rolling, together with excellent electrical conductivity.[3,4] However, due to the low packing density and large level of porosity of pure carbon materials (such as graphene), the areal or volumetric capacitance of these carbon-based materials is limited, usually not more than 100 mF cm^{-2}.[3,4] Thus, introduction of transition metal oxides/hydroxides[5–7] or conductive polymers[8,9] with pseudocapacitance has been regarded as a solution to further boost up the electrochemical performance of carbonaceous materials. By creating a hybrid nanocomposite of the flexible substrate, e.g., combining graphene or CNT paper with the pseudocapactive nanomaterials, such as MnO_x,[10,11] RuO_2,[12] polyaniline,[13] and polypyrrol,[14] the desired high conductivity could be coupled with pseudocapacitive nanomaterials for higher electrochemical performance, while retaining the structural flexibility.[5,10,11,15]

Among the mostly studied pseudocapacitive materials, MnO_x is environmental friendly, abundant, and has high theoretical capacitance.[16,17] Various carbonaceous materials/MnO_x hybrid nanocomposites, such as 3D network, core@shell, and 2D planer structures, have been synthesized and studied as electrodes for flexible supercapacitors recently.[5,10,11] In order to maintain the desired mechanical flexibility, the mass loading of the active materials has to be controlled, and at the same time to maximize the volumetric capacitance, energy, and power density.[6,11,15,18,19] Introduction of graphene material could potentially improve the loading amount of MnO_x; however, the poor dispersion of the metal oxides and restacking problems of the graphene can hinder the charge transfer ability and limit the energy and power densities. Thus, it is important to obtain good dispersion of the graphene and MnO_x hybrid and prevent restacking, so to maximize the energy and power densities for practical application.[20–22]

In the present work, Mn_3O_4 nanofibers are successfully assembled into 2D reduced-graphene oxide (rGO) paper by a facile hydrothermal method followed by electrochemical reduction. The Mn_3O_4 nanofiber gel obtained could be easily blended with graphene oxide (GO) suspension, thus a large amount of Mn_3O_4 could be loaded into the final nanohybrid paper with excellent dispersion. The electrical conductivity of this Mn_3O_4/rGO (MG) nanohybrid paper can be further improved by the electrochemical reduction followed, while retaining its mechanical flexibility and integrity. As a result, the unique hybrid nanocomposite structure generated a high mass loading of Mn_3O_4 at considerably small thickness (up to 2.13 mg cm^{-2} or 0.71 g cm^{-3}, equivalently), which is much higher than those of previously reported works.[5,10,11,15] When assembled into

Y. Hu, Dr. C. Guan, Dr. Q. Ke, Dr. X. Huang, Prof. J. Wang
Department of Materials Science and Engineering
National University of Singapore
9 Engineering Drive 1, 117576 Singapore
E-mail: msewangj@nus.edu.sg
G. Feng
Department of Chemical and Biomolecular Engineering
National University of Singapore
4 Engineering Drive 4, 117585 Singapore

DOI: 10.1002/adfm.201503528

flexible asymmetric supercapacitor (ASC) devices (operative in both neutral aqueous electrolyte and ionic liquid electrolyte), the highly conductive MG nanohybrid paper shows excellent electrochemical performance, such as high volumetric capacitance (54.6 F cm^{-3}), high energy and power density (0.0055 Wh cm^{-3} and 10.95 W cm^{-3}, respectively), and promising cycle ability (good performance up to 8000 cycles).

2. Results and Discussion

2.1. Electrochemical Reduction of MnO_x/GO Nanohybrid Paper

First, MnO_x nanofiber gels were obtained by a gel formation reaction, followed by growth of MnO_x nanocrystals within the GO suspension during hydrothermal reaction. The mixture is then assembled into a hybrid paper through facile vacuum filtration. Electrochemical reduction of GO-based material is a newly emerging technique to reduce GO in film or paper form, where there is no need for any reducing agents or high temperature being used.[23–25] It is much more environmental friendly and easy to scale up,[26–29] as compared to, for example, the high temperature thermal reduction and low temperature chemical reduction by acid or alkaline. This method was first used for graphene material in 2009.[25] By adjusting the external power source, the electronic states of the graphene oxide (as working electrode) could be effectively modified by changing the Fermi energy level.[25] Upon applying an appropriate voltage (e.g., negative potential −1.5 V), the energy barriers for oxygen functionalities is overcame. Thus, these electrochemically unstable oxygen groups are eliminated and the electrical insulating GO gradually becomes reduced to conductive graphene.[23]

The hybrid paper was reduced under a constant voltage of −1.5 V, for multiple cycles of 10 min each. **Figure 1**A shows the current versus time curves, indicating the reduced resistance as the current value increases for the first three cycles. The reduction is completed when the current becomes stable during the 4th cycle. To clearly understand the electrochemical reduction process, the impedance and cyclic voltammetry (CV) of the nanohybrid paper were tested after each cycle (Figure 1B–D). The successful reduction was illustrated by the impedance test, as shown in Figure 1B, where one could see that the internal resistance of the hybrid paper dramatically dropped upon reduction. The capacitance of the hybrid paper increased from 6.23 to 86.0 F cm^{-3} after a facile 30 min reduction (Figure 1D), further confirmed the effectiveness of electrochemical reduction.

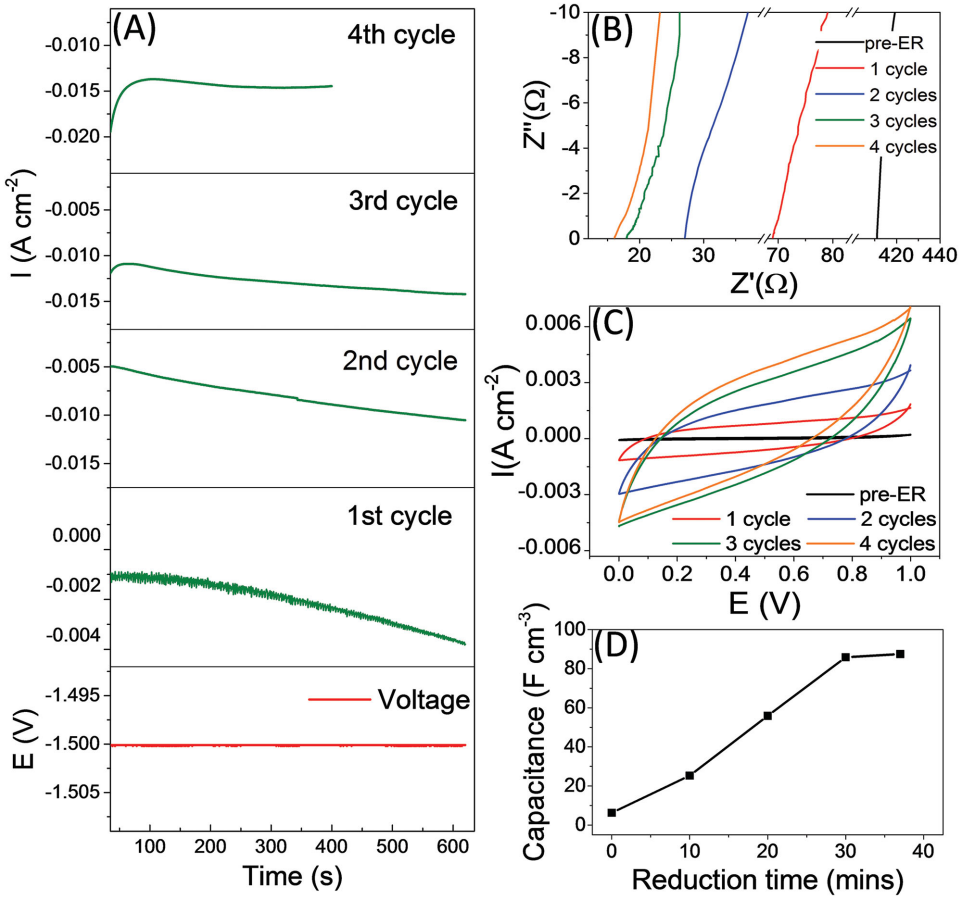

Figure 1. Electrochemical reduction results: A) current and voltage curves during multiple cycles of electrochemical reduction; B) Nyquist plot of MG nanohybrid paper after various cycles of electrochemical reduction; C) CV curves of the MG nanohybrid paper after various cycles of electrochemical reduction under 10 mV s^{-1} scan rate; and D) volumetric capacitance calculated from CV tests (10 mV s^{-1} scan rate) after various numbers of cycles of electrochemical reduction (i.e., reduction time).

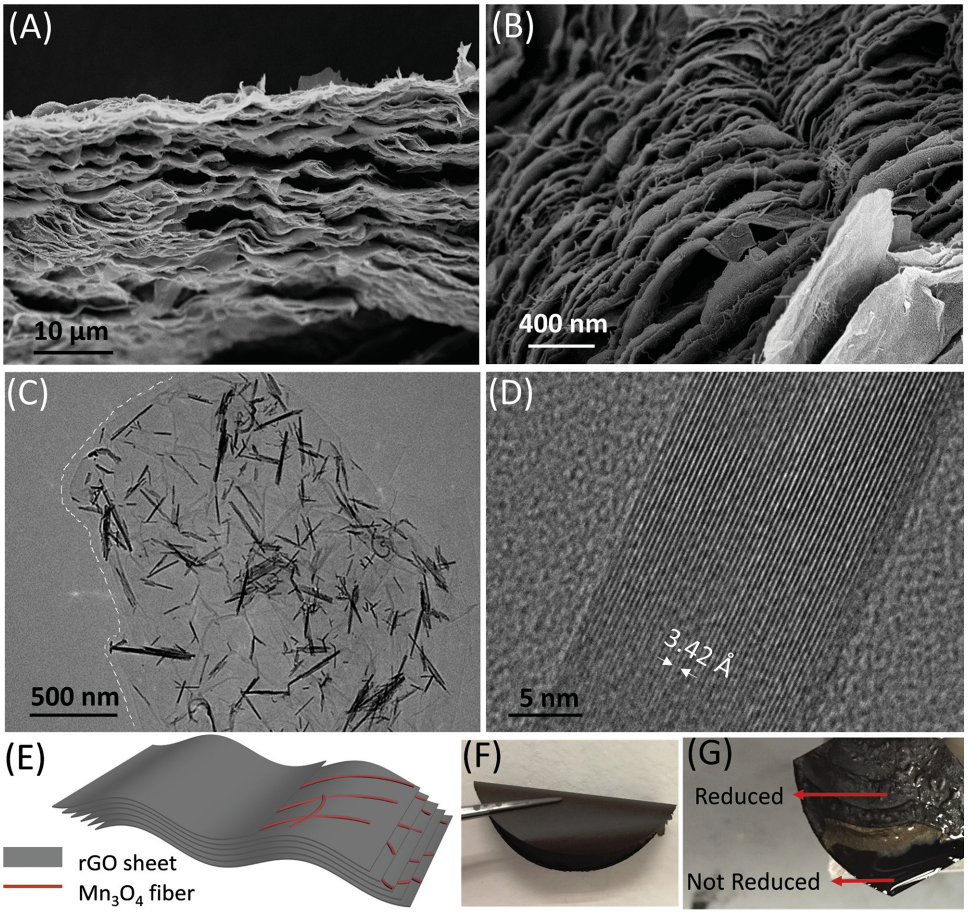

Figure 2. SEM images of MG nanohybrid paper: A) from cross-sectional view and B) higher magnification from side view. TEM images of C) MnO_x nanofibers embedded in a rGO sheet, with part of the rGO sheet's edge marked out and D) high magnification of MnO_x with lattice fringe spacing. E) Schematic diagram showing how MnO_x nanofibers are embedded among rGO sheets. Pictures of F) as filtered MnO_x/GO nanohybrid paper rolled freely and G) top view of as-reduced MG nanohybrid paper.

The morphologies and detailed structures of MG nanohybrid paper were characterized using both scanning electron microscopy (SEM) and transmission electron microscopy (TEM). The nanohybrid paper consists of hundreds of layers of rGO sheets (**Figure 2**A). Among the individual rGO sheets, lay the well dispersed MnO_x nanofibers (Figure 2B), which ensure good charge transfer ability through the highly conductive graphene channels.[30] The MnO_x nanofibers are loosely bonded, as shown by the TEM image, where the nanofibers are 300–500 nm in length and evenly distributed within the rGO sheets (Figure 2C). High resolution TEM image (Figure 2D) reveals the lattice fringe of 0.342 nm and the dimension of the MnO_x nanofibers (≈17 nm). Figure 2E shows a schematic drawing illustrating how the MnO_x nanofibers are embedded among rGO sheets and the resulted flexible nanohybrid paper. The excellent dispersion is benefited from the MnO_x gel, which could mix freely with the GO suspension. This structure, in which the MnO_x nanofibers also act as spacers among the individual GO sheets (as shown in the SEM image and scheme of Figure 2B,E), eliminates the restacking problem of the individual rGO sheets, which were encountered in most well-established processes (e.g., Hummer's method).[31,32] Specifically, restacking during reduction and drying process cause a reduction in effective surface area for charge storage which limits the specific capacitance for the graphene-based materials (100–120 F g^{-1}).[33–35]

rGO paper is also prepared and reduced by the same method discussed above (i.e., vacuum filtration and electrochemical reduction). Figure S1B (Supporting Information) and Figure 2F show the as-filtered GO and MnO_x/GO nanohybrid paper, respectively. The GO paper exhibited a darker color and appeared to be crispier and thinner than MnO_x/GO nanohybrid paper, due to the MnO_x nanofiber doped in the MnO_x/GO nanohybrid paper. However, both papers could be freely rolled, showing their high mechanical flexibility, even after reduction (Figure S1C,D, Supporting Information). Figure 2G shows that the electrochemically reduced part of the MG nanohybrid paper appears to have some geometric wrinkling. These are caused by interlocking among the rGO sheets, which results into better mechanical properties and lower surface energy.[23] In addition, they give rise to high surface area and specific capacitance.[36] Similarly, this phenomenon happens to the rGO sheets obtained from other processes, e.g., chemical or thermal reduction.[33,37] The color change of the reduced part, compared to the nonreduced part, indicates an improved charge transport properties.[24]

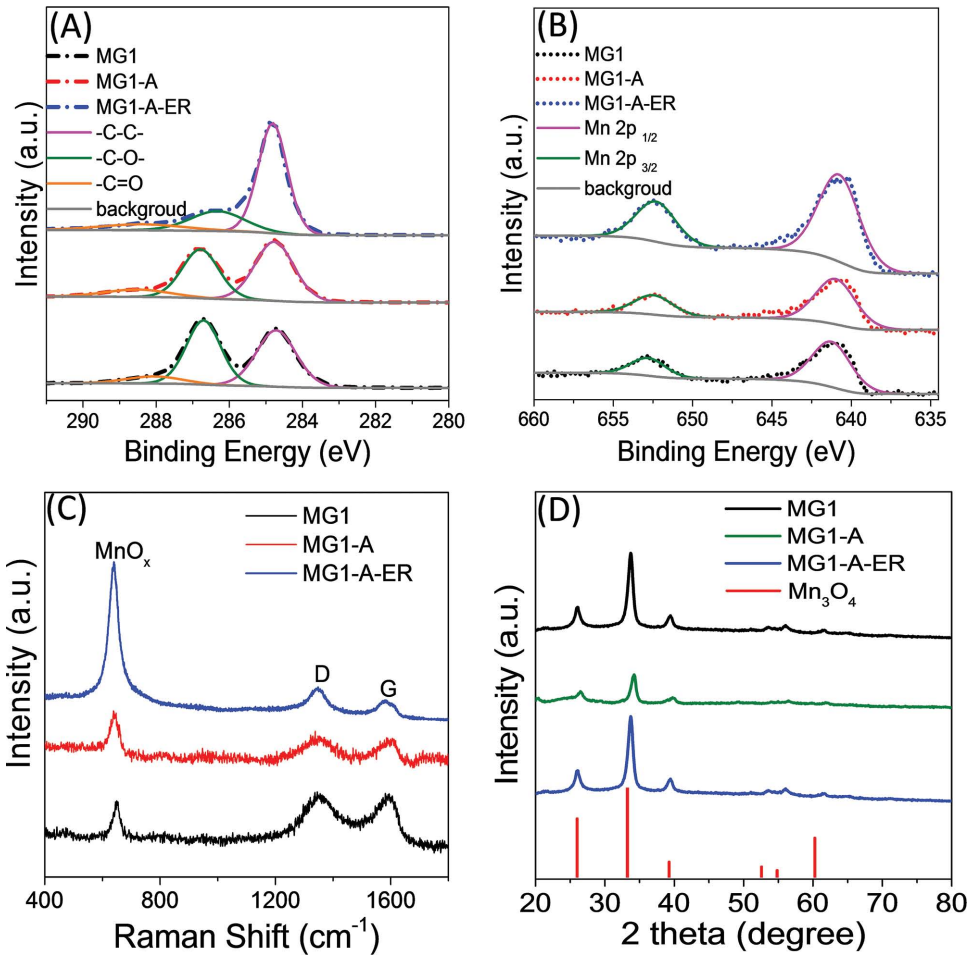

Figure 3. XPS spectra and peak fitting of the samples MG1 (as filtered MnO_x/GO nanohybrid paper), MG1-A (annealed MnO_x/GO nanohybrid paper) and MG1-A-ER (electrochemically reduced MG nanohybrid paper after annealing) for A) C 1_s and B) Mn 2_p. C) Raman spectra for the samples MG1, MG1-A, and MG1-A-ER; D) XRD patterns of the samples MG1, MG1-A, and MG1-A-ER.

2.2. Characterizations of MG Nanohybrid Paper

In order to further study the effect of reduction, characterizations are conducted for the as filtered MnO_x/GO nanohybrid paper (sample MG1), the annealed MnO_x/GO nanohybrid paper (sample MG1-A, annealed in N_2 atmosphere at 150 °C to eliminate moisture and to enhance mechanical strength) and the electrochemically reduced MG nanohybrid paper after annealing (sample MG1-A-ER). GO is electrically insulating, as the large amount of saturated sp^3 bonds and electronegative oxygen atoms bonded to carbon give rise to an energy gap in the electron density of states.[38] Therefore, it is essential to reduce it and restore its conjugated carbon network and electrical conductivity, for electrochemical application. **Figure 3**A shows the X-ray photoelectron spectroscopy (XPS) spectra for C 1s of the three samples. After reduction (sample MG1-A-ER), the –C–O– to –C–C ratio is largely reduced, indicating the elimination of oxygen functional groups, as mentioned above. The –C–C– peak becomes dominating, indicating the GO becomes into graphene.[24] The effect of the mild annealing on the –C–O– to –C–C– ratio is negligible. Figure 3B shows the XPS spectra of Mn 2p for the three samples. For all three samples, peaks of Mn $2p_{3/2}$ and Mn $2p_{1/2}$ are centered at 640.8 and 652.4 eV, respectively, which are in good agreement with the XPS data reported for peaks of Mn $2p_{3/2}$ and Mn $2p_{1/2}$ in mixed valence Mn_3O_4.[39] Therefore, the chemical states of the MnO_x nanofibers are Mn_3O_4. The redox reactions between the III and IV oxidation states of Mn ions occurs spontaneously during the charge–discharge process.[40] Both MnO_2 and Mn_3O_4 have been widely studied for electrochemical applications, as they are showing the best electrochemical performances among the various manganese oxides (MnO, Mn_2O_3, Mn_3O_4, and MnO_2).[41,42] In addition, the unchanged peak positions in Figure 3B indicate that the electrochemical reduction did not change the chemical state of the Mn_3O_4 nanofibers. Figure S2 (Supporting Information) demonstrates the XPS spectra for C 1s for the GO paper, the annealed GO paper and the electrochemically reduced GO (rGO) paper, which show similar phenomenon as the MG nanohybrid paper.

Raman spectra show the D and G band of the nanohybrid papers (Figure 3C). The D band located at 1350 cm^{-1} and the G band at 1595 cm^{-1} are characteristic Raman shifts of graphite,

which can be observed in the Raman spectra of MG nanohybrid papers before and after annealing or reduction (sample MG1, MG1-A, and MG1-A-ER). Upon reduction, the relative intensity of D band peak only increased slightly compared to the unreduced MnO_x/GO nanohybrid paper, due to the defects introduced by reduction.[25] However, the MnO_x peak at ≈630 cm^{-1} became much higher compared to carbon peaks, indicating the relative Mn_3O_4 content had increased. Thermal gravimetric analysis (TGA) results (Figure S1E, Supporting Information) further confirmed that the Mn_3O_4 content increased from 36.5 to 49.0 wt% upon reduction. This is mainly due to the elimination of the oxygen groups, as mentioned earlier. X-ray diffraction (XRD) patterns show the well match of peak positions of the nanohybrid papers with the powder diffraction file (PDF) of Mn_3O_4 crystal structure (Figure 3D). This further confirms the chemical states of nanofibers as Mn_3O_4, and that the electrochemical reduction is an effective way of reducing GO, without affecting the chemical states of the embedded Mn_3O_4 nanofibers. The d-spacing of (220) plane of Mn_3O_4 crystal structure (PDF:01-086-2337) is consistent with the lattice fringe measurement (Figure 1D).

2.3. Electrochemical Performance of MG/rGO ASC

Upon the electrochemical reduction, the MG nanohybrid paper and the rGO paper were then assembled into ASC. An ASC consists of a battery-type Faradaic electrode as the energy source (cathode) and a capacitor-type electrode as the power source (anode),[43] e.g., a combination of a carbon-based material as the anode with a pseudocapacitive MnO_2-based cathode, which can extend the voltage window up to 2 V in aqueous electrolytes.[44] ASC have been found to be an effective approach for development of high energy and power density supercapacitors, through providing enlarged voltage window and specific capacitance of active materials.[45] It also overcomes the limitation of voltage window caused by water decomposition at 1.23 V, when the individual voltage windows for the cathode and anode are well separated.[46] This greatly improves the energy and power density, compare to symmetric supercapacitors (MnO_x's voltage window is capped at 1 V when tested as symmetric supercapacitors in aqueous electrolytes).[47,48]

2.3.1. In Aqueous Electrolyte

The ASC was first prepared using 1 M Na_2SO_4 as the aqueous electrolyte. By characterizing the two papers (MG nanohybrid paper and rGO paper) individually in 1 M Na_2SO_4 aqueous electrolyte, it is shown that the effective voltage window for MG nanohybrid paper is from 0 to 1.0 V, while for rGO paper is from −1.0 to 0 V (Figure S3, Supporting Information). Therefore, the ASC based on MG nanohybrid paper as the cathode, rGO paper as the anode is expected to have a 2 V voltage window in the aqueous electrolyte.[24] Several cathode samples are compared (while same rGO paper is used as anode for all ASCs), namely, MG nanohybrid paper that is thermally reduced (sample MG1-TR), MG nanohybrid paper that is electrochemically reduced without prereduction annealing (sample MG1-ER), MG nanohybrid paper with 3 wt% CNT being added

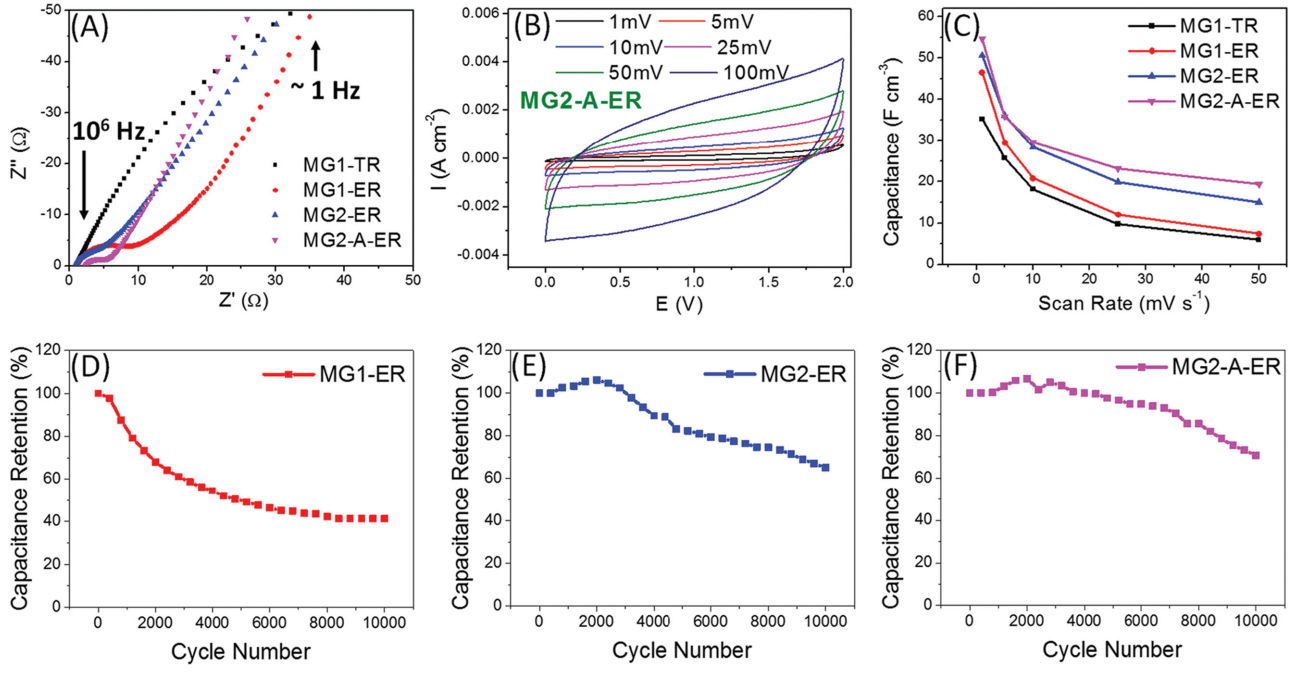

Figure 4. Electrochemical characterizations in an aqueous electrolyte for MG1-TR (thermally reduced MG nanohybrid paper), MG1-ER (electrochemically reduced MG nanohybrid paper), MG2-ER (MG nanohybrid paper with 3 wt% CNT), and MG2-A-ER (MG nanohybrid paper with 3 wt% CNT and prereduction annealing): A) Nyquist plots of various samples; B) CV curves at different scan rates (1, 5, 10, 25, 50, and 100 mV s^{-1}) for the sample MG2-A-ER; C) comparison of the volumetric capacitance of various samples at different scan rates; cycling ability results at 2 A g^{-1} of charge–discharge tests for D) MG1-ER, E) MG2-ER, and F) MG2-A-ER.

before vacuum filtration and is electrochemically reduced, with or without prereduction annealing (sample MG2-ER and sample MG2-A-ER). Among the established reduction methods for rGO, thermal reduction at elevated temperature is proven to be able to reduce individual GO platelets or sheets, without using reducing agents.[38,49] CNT is added during the gel formation step as CNT is known to enhance the mechanical strength and electrical conductivity.[15,50,51]

Impedance tests results show that sample MG1-ER has a much smaller semicircle and higher slope of the Nyquist plot than that of sample MG1-TR (**Figure 4**A and Figure S4A, Supporting Information), although the internal resistance is similar. This indicates that electrochemically reduced MG nanohybrid paper exhibits a much lower charge carrier resistance than that of the thermally reduced one.[52,53] From the CV test results, sample MG1-ER shows much more rectangular and symmetrical CV loops than MG1-TR, at all scan rates (Figures S5 and S6, Supporting Information). It is known that a perfect rectangular CV response correlates to better capacitive behavior, specifically, a continuous and reversible faradaic reaction of the manganese oxide.[54] Thus, sample MG1-ER shows a higher volumetric capacitance than that of sample MG1-TR (Figure 4C). Therefore, the electrochemically reduced MG nanohybrid paper is much more conductive and electroaccessible than the thermally reduced MG paper, making it a better capacitive electrode.[55] It is known that MnO_x materials do not often show redox peaks in their CV curves, as the pseudocapacitive charge storage for MnO_x is based on successive multiple surface redox reactions.[56] In addition, the symmetric and rectangular CV curves also indicate that there is no signs of water decomposition above 1.23 V.[57]

Upon adding CNTs, the radiance of the Nyquist semicircle becomes smaller for sample MG2-ER as compared to that of sample MG1-ER (Figure 4A). This indicates that the charge-transfer ability is improved by the CNTs added.[53] The CV loops of sample MG2-ER and sample MG1-ER show similar shapes and the calculated volumetric capacitance only improved about 9% (46.6–50.7 F cm^{-3} at 1 mV s^{-1}). However, upon adding CNTs, the rate capability improved (Figure 4C) as the volumetric capacitance at 100 mV s^{-1} improved 100% upon adding CNT. Therefore, CNT improved the charge transfer ability of sample MG2-ER, which caused the slowing down of faradaic reaction at higher scan rate becoming less obvious.[53]

Sample MG2-A-ER, which went through prereduction annealing, shows the highest slope and a perfect straight line in lower frequency region of Nyquist plot (Figure 4A), indicating a lower ion diffusion resistance as compare to sample MG2-ER. This is due to the more uniform reduction upon pre-ER annealing (the preannealed samples show no ripples of color changes unlike the nonannealed one in Figure 1G). Therefore, prereduction annealing is necessary for better electrochemical reduction and results in highest volumetric capacitance and rate capability (Figure 4C). The highest volumetric capacitance of 54.6 F cm^{-3} (equivalent to 546.05 mF cm^{-2}) in 1 M Na_2SO_4 is obtained at 1 mV s^{-1} scan rate of CV test, which is obviously much higher than those reported for MnO_x-based ASC devices (Table S1, Supporting Information). In addition, the symmetrical and near rectangular CV shape of sample MG2-A-ER indicate a good capacitive behavior, as shown in Figure 4B. The high volumetric capacitance obtained is mainly contributed by the high mass loading (0.21 g cm^{-3} in the full ASC device) of Mn_3O_4 nanofibers, well dispersion of crystallized Mn_3O_4 nanofibers within the rGO sheets and much hindered restacking of the rGO sheets, which lead to much improved accessibility by electrolytes and charge transfers.

The cycle ability is evaluated at 2 A g^{-1} current density of the charge–discharge test for sample MG1-ER, MG2-ER, and MG2-A-ER. Figure 4D–F shows that the two MG nanohybrid papers with CNT being added, demonstrate the activation phenomenon and much better cycle ability, when compare to the one without CNT. CNT appears to help preserve the desired nanostructure of metal oxides during cyclings,[58] where the Mn_3O_4 nanofibers and CNTs are well mixed and well dispersed among each other (Figure S1A, Supporting Information). This hybrid structure plays an important role in preventing the Mn_3O_4 nanofibers from thickening and greatly improved the cycling ability of the device. Sample MG2-A-ER shows excellent cycle ability of 95% retention after 6000 cycles and about 85% retention after 8000 cycles. The samples are tested for galvanostatic charge–discharge at various current densities. Figure S7 (Supporting Information) shows the charge–discharge curve at current densities of 1, 2, 5, and 10 A cm^{-3}, for sample MG2-A-ER. A high columbic efficiency is obtained at the current density of 1 A cm^{-3} (98.3%), calculated on the basis of charge and discharge time.[59]

2.3.2. In Ionic Liquid Electrolyte

To study the electrochemical performances in ionic liquid electrolyte, a flexible ASC is assembled using the flexible packaging and ionic electrolyte, 1 M 1-ethyl-3-methylimidazolium tetrafluoroborate ($EMIMBF_4$) in acetone nitrile solution. Such ionic liquid electrolyte could provide much wider window due to its high decomposition voltage compared to that of water in aqueous electrolyte (0–3 V in this case).[60,61] **Figure 5**C shows the schematic illustration of the flexible ASC device based on MG nanohybrid paper as the cathode and rGO paper as the anode in the 1 M $EMIMBF_4$ in acetone nitrile ionic liquid electrolyte, wrapped in a flexible packaging. Figure 5D–F shows the top view and side views of the ASC and bended ASC, demonstrating its mechanical flexibility. Sample MG2-A-ER is evaluated in flexible ASC packaging with ionic liquid electrolyte inside (sample MG2-A-ER-IL) at different bending angles (Figure 5A). However, the CV curves of sample MG2-A-ER-IL at bending angels of 60°, 120°, and 180° under the scan rate of 5 mV s^{-1} all showing less rectangular shapes but an oval one, compare to that of sample MG2-A-ER tested in aqueous electrolyte (Figures 4A and 5A). The volumetric capacitance is also lower than that of the ASC tested in aqueous electrolyte. These indicate that such spinel-structure Mn_3O_4 nanohybrid paper has better capacitive behavior in aqueous electrolyte. One possible reason could well be that the cations in $EMIMBF_4$ are too big to tunnel through the Mn_3O_4 octahedrons, thus the redox reaction could only take place on the surface of the Mn_3O_4 nanofibers.[41,62] CV curves and calculted capacitance for sample MG2-A-ER-IL show that, when bended (Figure 5A and insert), the capacitance is not affected much, demonstrating its excellent mechanical flexibility. Due to the wide voltage window

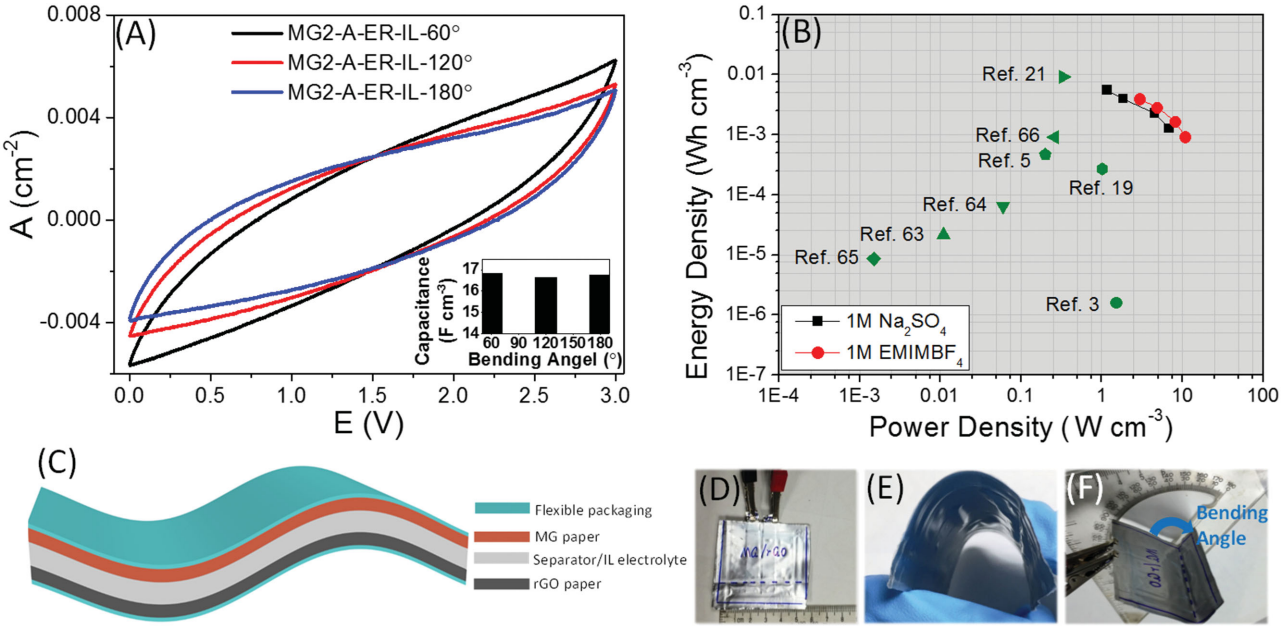

Figure 5. Electrochemical studies in flexible ASCs using an ionic liquid electrolyte: A) CV curves collected at different bending angles in an ionic liquid electrolyte under a scan rate of 5 mV s^{-1}. Inset: calculated volumetric capacitance at a scan rate of 1 mV s^{-1}; B) Ragone plot of the ASC devices measured in both aqueous and ionic liquid electrolyte, and the values reported for other supercapacitor devices are compared within the graph; C) schematic illustration of the flexible ASC device based on MG nanohybrid paper as the positive electrode and rGO paper as the negative electrode in a diluted ionic liquid (1 M $EMIMBF_4$ in acetone nitrile) electrolyte, wrapped in a flexible packaging; pictures of D) top view of the flexible ASC device; E) side view of the freely bended ASC device, and F) ASC bended to a certain angle while testing electrochemical performances.

of the ionic liquid electrolyte, the calculated energy and power density are comparable with the ASC tested in aqueous electrolyte (Figure 5B).

When evaluated in aqueous electrolyte, the highest volumetric energy and power density obtained are 0.0055 Wh cm^{-3} (at corresponding power density of 1.15 W cm^{-3}) and 6.86 W cm^{-3} (at corresponding energy density of 0.0013 Wh cm^{-3}), respectively. For the ASC tested in ionic liquid electrolyte, the highest volumetric energy and power density obtained are 0.0039 Wh cm^{-3} (at the corresponding power density of 2.94 W cm^{-3}) and 10.95 W cm^{-3} (at the corresponding energy density of 0.0009 Wh cm^{-3}), respectively. It was noted that the volume used for calculation included the volume of the cathode, anode, and the separator. For comparison purposes, these values are plotted in the Ragone plot together with the values from other reports of supercapacitors (mostly MnO_x-based ASC devices).[3,5,19,21,63–66] To the best of our knowledge, this excellent performance is among the best in terms of capacitance, cycling ability, energy density, and power density, for mechanically flexible MnO_x-based ASC devices.[3,10,19,21,64,67–70]

3. Conclusion

A novel nanocomposite-type MnO_x/rGO hybrid paper is prepared by facile and convenient techniques (gel formation and electrochemical reduction), by which highly crystallized Mn_3O_4 nanofibers are well integrated within a highly conductive and mechanically flexible rGO paper, which can effectively accelerate the charge transfer for a fast pseudoreaction even with high mass loading. Flexible ASC devices using a Mn_3O_4/rGO nanohybrid paper and a rGO paper were assembled and studied in both aqueous and ionic liquid electrolytes, which demonstrated an outstanding volumetric capacitance of 54.6 F cm^{-3} and energy and power densities of 0.0055 Wh cm^{-3} and 10.95 W cm^{-3}, respectively. The high volumetric power density, to the best of our knowledge, is the highest among the reported results for MnO_x-based flexible ASC devices. In addition, the cell also showed excellent cycling ability with 95% of capacitance being maintained after 6000 cycles, which is superior among MnO_x-based supercapacitors. The facile preparation method and the high performance of the Mn_3O_4/rGO nanohybrid paper deserve further exploration for next generation flexible devices of energy and power sources.

4. Experimental Section

Material Synthesis: Pyrrole was added into 0.2 M $KMnO_4$ dropwise. A gel was then formed. The gel is washed three times to remove the unreacted $KMnO_4$ solution and polypyrrole formed from the redox reaction. GO aqueous dispersion of 5 g L^{-1} (Graphene Laboratories Inc.) was added into the washed gel. The mixture was then stirred for at least 12 h and undergone hydrothermal reaction at 85 °C for 12 h. More GO dispersion was added into the product from hydrothermal reaction. The solution is stirred well before undergoing vacuum filtration. For GO paper, GO dispersion was diluted by distilled water and then undergone vacuum filtration. The filtered paper was then thermally annealed in N_2 atmosphere at 150 °C for 30 min to eliminate water and to enhance mechanical strength.

Electrochemical and Thermal Reduction: Electrochemical reduction of the annealed GO or Mn_3O_4/GO nanohybrid paper as the working electrode was performed in 0.1 M Na_2SO_4 aqueous solution at the

potential of –1.5 V for a few cycles, each cycle for 600 s. A Pt plate and Ag/AgCl electrode were used as the counter electrode and the reference electrode, respectively. The reduced paper was then washed and dried. Electrochemical measurements after each reduction cycle were also carried out in this setting. Thermal reduction was conducted in an air flowing oven, in which the GO or MG paper was heated at 200 °C for 5 h.

Materials Characterizations: XRD patterns were collected on a Bruker's X-ray powder diffractometer (D8 Advance, Cu Kα, λ = 0.154 nm). XPS studies were conducted with a Kratos' Axis Ultra DLD (delay line detector) photoelectron spectrometer. Transmission electron microscopy (JOEL 2010F, 200 kV) and field-emission scanning electron microscopy (SUPRA 40 ZEISS, Germany) were used to examine the morphology of all samples. Raman scattering spectra were recorded on a LABRAM-HR Raman spectrometer excited with 514.5 nm Ar+ laser. Mass content were measured by thermal gravimetric analysis (SDT Q600).

Electrochemical Measurements: A piece of MG nanohybrid paper and rGO paper were used as the cathode material and anode material, respectively. After matching their capacitance (through adjusting the size of the MG nanohybrid or rGO paper), the two papers were assembled into aluminum soft packing for capacitance and impedance tests in aqueous electrolyte or ionic liquid electrolyte (1 M 1-ethyl-3-methylimidazolium tetrafluoroborate ($C_6H_{11}BF_4N_2$, 04365, [143314-16-3]) in acetone nitrile solution). CV, galvanostatic charge/discharge (C/D) measurement, and electrical impedance spectroscopy were conducted using Solartron System 1470E and 1400A, respectively. For both CV and C/D, the measurement voltage was controlled in the range of 0–2 V for aqueous electrolyte test and 0–3 V for ionic liquid electrolyte test. Scan rates of 1, 5, 10, 25, 50, and 100 mV s^{-1} were used for CV, while the current densities of 1, 2, 5, and 10 A cm^{-3} were used for C/D measurement. The areal loading of Mn_3O_4/GO, Mn_3O_4/rGO nanohybrid paper, and rGO paper are 6.34, 4.34, and 2.0 mg cm^{-2}, respectively. The thickness of Mn_3O_4/rGO nanohybrid paper, rGO paper, and the separator used for the ASCs are 29, 20, and 52 μm, respectively. The area of cathode and anode is controlled at 1–2 cm^2. The frequency for impedance test is from 10^6 to 0.1 Hz.

Supporting Information

Supporting Information is available from the Wiley Online Library or from the author.

Acknowledgements

This work was supported by Singapore MOE (Ministry of Education), Tier 2, MOE2012-T2-2-102, conducted at the National University of Singapore.

Received: August 20, 2015
Revised: September 22, 2015
Published online: November 5, 2015

[1] X. Lu, M. Yu, G. Wang, Y. Tong, Y. Li, *Energy Environ. Sci.* **2014**, *7*, 2160.
[2] X. Peng, L. Peng, C. Wu, Y. Xie, *Chem. Soc. Rev.* **2014***43*, 3303.
[3] M. F. El-Kady, V. Strong, S. Dubin, R. B. Kaner, *Science* **2012**, *335*, 1326.
[4] Y. Xu, Z. Lin, X. Huang, Y. Liu, Y. Huang, X. Duan, *ACS Nano* **2013**, *7*, 4042.
[5] X. Lu, M. Yu, G. Wang, T. Zhai, S. Xie, Y. Ling, Y. Tong, Y. Li, *Adv. Mater.* **2013**, *25*, 267.
[6] X. Lu, T. Zhai, X. Zhang, Y. Shen, L. Yuan, B. Hu, L. Gong, J. Chen, Y. Gao, J. Zhou, Y. Tong, Z. L. Wang, *Adv. Mater.* **2012**, *24*, 938.
[7] J. Xie, X. Sun, N. Zhang, K. Xu, M. Zhou, Y. Xie, *Nano Energy* **2013**, *2*, 65.
[8] C. Meng, C. Liu, L. Chen, C. Hu, S. Fan, *Nano Lett.* **2010**, *10*, 4025.
[9] L. Yuan, X. Xiao, T. Ding, J. Zhong, X. Zhang, Y. Shen, B. Hu, Y. Huang, J. Zhou, Z. L. Wang, *Angew. Chem. Int. Ed.* **2012**, *51*, 4934.
[10] L. Peng, X. Peng, B. Liu, C. Wu, Y. Xie, G. Yu, *Nano Lett.* **2013**, *13*, 2151.
[11] Y. He, W. Chen, X. Li, Z. Zhang, J. Fu, C. Zhao, E. Xie, *ACS Nano* **2013**, *7*, 174.
[12] B. G. Choi, S.-J. Chang, H.-W. Kang, C. P. Park, H. J. Kim, W. H. Hong, S. Lee, Y. S. Huh, *Nanoscale* **2012**, *4*, 4983.
[13] H.-P. Cong, X.-C. Ren, P. Wang, S.-H. Yu, *Energy Environ. Sci.* **2013**, *6*, 1185.
[14] X. Lu, H. Dou, C. Yuan, S. Yang, L. Hao, F. Zhang, L. Shen, L. Zhang, X. Zhang, *J. Power Sources* **2012**, *197*, 319.
[15] Y. Cheng, S. Lu, H. Zhang, C. V. Varanasi, J. Liu, *Nano Lett.* **2012**, *12*, 4206.
[16] G. Wang, L. Zhang, J. Zhang, *Chem. Soc. Rev.* **2012**, *41*, 797.
[17] K. Zhang, X. Han, Z. Hu, X. Zhang, Z. Tao, J. Chen, *Chem. Soc. Rev.* **2014**, *44*, 699.
[18] P. Yang, X. Xiao, Y. Li, Y. Ding, P. Qiang, X. Tan, W. Mai, Z. Lin, W. Wu, T. Li, H. Jin, P. Liu, J. Zhou, C. P. Wong, Z. L. Wang, *ACS Nano* **2013**, *7*, 2617.
[19] T. Zhai, S. Xie, M. Yu, P. Fang, C. Liang, X. Lu, Y. Tong, *Nano Energy* **2014**, *8*, 255.
[20] Y. Cheng, H. Zhang, S. Lu, C. V. Varanasi, J. Liu, *Nanoscale* **2013**, *5*, 1067.
[21] J. Liu, L. Zhang, H. B. Wu, J. Lin, Z. Shen, X. W. Lou, *Energy Environ. Sci.* **2014**, *7*, 3709.
[22] T. Zhai, F. Wang, M. Yu, S. Xie, C. Liang, C. Li, F. Xiao, R. Tang, Q. Wu, X. Lu, Y. Tong, *Nanoscale* **2013**, *5*, 6790.
[23] J. Yang, S. Gunasekaran, *Carbon* **2013**, *51*, 36.
[24] Z. Zhang, F. Xiao, L. Qian, J. Xiao, S. Wang, Y. Liu, *Adv. Energy Mater.* **2014**, *4*, n/a.
[25] H.-L. Guo, X.-F. Wang, Q.-Y. Qian, F.-B. Wang, X.-H. Xia, *ACS Nano* **2009**, *3*, 2653.
[26] X. Wang, L. Zhi, K. Müllen, *Nano Lett.* **2008**, *8*, 323.
[27] H. A. Becerril, J. Mao, Z. Liu, R. M. Stoltenberg, Z. Bao, Y. Chen, *ACS Nano* **2008**, *2*, 463.
[28] S. Pei, J. Zhao, J. Du, W. Ren, H.-M. Cheng, *Carbon* **2010**, *48*, 4466.
[29] X. Fan, W. Peng, Y. Li, X. Li, S. Wang, G. Zhang, F. Zhang, *Adv. Mater.* **2008**, *20*, 4490.
[30] J. Chang, M. Jin, F. Yao, T. H. Kim, V. T. Le, H. Yue, F. Gunes, B. Li, A. Ghosh, S. Xie, Y. H. Lee, *Adv. Funct. Mater.* **2013**, *23*, 5074.
[31] J. H. Lee, N. Park, B. G. Kim, D. S. Jung, K. Im, J. Hur, J. W. Choi, *ACS Nano* **2013**, *7*, 9366.
[32] Q. Ke, Y. Liu, H. Liu, Y. Zhang, Y. Hu, J. Wang, *RSC Adv.* **2014**, *4*, 26398.
[33] Y. Zhu, M. D. Stoller, W. Cai, A. Velamakanni, R. D. Piner, D. Chen, R. S. Ruoff, *ACS Nano* **2010**, *4*, 1227.
[34] Z. Wen, X. Wang, S. Mao, Z. Bo, H. Kim, S. Cui, G. Lu, X. Feng, J. Chen, *Adv. Mater.* **2012**, *24*, 5610.
[35] H. M. Jeong, J. W. Lee, W. H. Shin, Y. J. Choi, H. J. Shin, J. K. Kang, J. W. Choi, *Nano Lett.* **2011**, *11*, 2472.
[36] Z. Chen, W. Ren, L. Gao, B. Liu, S. Pei, H.-M. Cheng, *Nat. Mater.* **2011**, *10*, 424.
[37] E.-Y. Choi, T. H. Han, J. Hong, J. E. Kim, S. H. Lee, H. W. Kim, S. O. Kim, *J. Mater. Chem.* **2010**, *20*, 1907.
[38] I. Jung, D. A. Dikin, R. D. Piner, R. S. Ruoff, *Nano Lett.* **2008**, *8*, 4283.
[39] A. Moses Ezhil Raj, S. G. Victoria, V. B. Jothy, C. Ravidhas, J. Wollschläger, M. Suendorf, M. Neumann, M. Jayachandran, C. Sanjeeviraja, *Appl. Surf. Sci.* **2010**, *256*, 2920.

[40] Q. Jiangying, G. Feng, Z. Quan, W. Zhiyu, H. Han, L. Beibei, W. Wubo, W. Xuzhen, Q. Jieshan, *Nanoscale* **2013**, *5*, 2999.
[41] W. Wei, X. Cui, W. Chen, D. G. Ivey, *Chem. Soc. Rev.* **2011**, *40*, 1697.
[42] Y. Hu, J. Wang, *J. Power Sources* **2015**, *286*, 394.
[43] Z.-S. Wu, W. Ren, D.-W. Wang, F. Li, B. Liu, H.-M. Cheng, *ACS Nano* **2010**, *4*, 5835.
[44] V. Khomenko, E. Raymundo-Piñero, F. Béguin, *J. Power Sources* **2006**, *153*, 183.
[45] J. Yan, Z. Fan, W. Sun, G. Ning, T. Wei, Q. Zhang, R. Zhang, L. Zhi, F. Wei, *Adv. Funct. Mater.* **2012**, *22*, 2632.
[46] K. C. Ng, S. Zhang, C. Peng, G. Z. Chen, *J. Electrochem. Soc.* **2009**, *156*, A846.
[47] Q. Li, Z.-L. Wang, G.-R. Li, R. Guo, L.-X. Ding, Y.-X. Tong, *Nano Lett.* **2012**, *12*, 3803.
[48] M.-J. Deng, P.-J. Ho, C.-Z. Song, S.-A. Chen, J.-F. Lee, J.-M. Chen, K.-T. Lu, *Energy Environ. Sci.* **2013**, *6*, 2178.
[49] M. Toupin, T. Brousse, D. Bélanger, *Chem. Mater.* **2004**, *16*, 3184.
[50] W. Lu, M. Zu, J.-H. Byun, B.-S. Kim, T.-W. Chou, *Adv. Mater.* **2012**, *24*, 1805.
[51] X. Chen, X. Chen, F. Zhang, Z. Yang, S. Huang, *J. Power Sources* **2013**, *243*, 555.
[52] H. Yoo, M. Min, S. Bak, Y. Yoon, H. Lee, *J. Mater. Chem. A* **2014**, *2*, 6663.
[53] C. Guan, J. Liu, Y. Wang, L. Mao, Z. Fan, Z. Shen, H. Zhang, J. Wang, *ACS Nano* **2015**, *9*, 5198.
[54] D. P. Dubal, D. Aradilla, G. Bidan, P. Gentile, T. J. S. Schubert, J. Wimberg, S. Sadki, P. Gomez-Romero, *Sci. Rep.* **2015**, DOI: 10.1038/srep09771.
[55] H.-W. Chang, Y.-R. Lu, J.-L. Chen, C.-L. Chen, J.-F. Lee, J.-M. Chen, Y.-C. Tsai, C.-M. Chang, P.-H. Yeh, W.-C. Chou, Y.-H. Liou, C.-L. Dong, *Nanoscale* **2015**, *7*, 1725.
[56] P. Simon, Y. Gogotsi, *Nat. Mater.* **2008**, *7*, 845.
[57] H. Xia, B. Li, L. Lu, *RSC Adv.* **2014**, *4*, 11111.
[58] P. Wu, N. Du, H. Zhang, J. Yu, D. Yang, *J. Phys. Chem. C* **2010**, *114*, 22535.
[59] Jaidev, R. I. Jafri, A. K. Mishra, S. Ramaprabhu, *J. Mater. Chem.* **2011**, *21*, 17601.
[60] J. Fuller, R. T. Carlin, R. A. Osteryoung, *J. Electrochem. Soc.* **1997**, *144*, 3881.
[61] M. M. Hantel, A. Płatek, T. Kaspar, R. Nesper, A. Wokaun, R. Kötz, *Electrochim. Acta* **2013**, *110*, 234.
[62] L. L. Zhang, X. S. Zhao, *Chem. Soc. Rev.* **2009**, *38*, 2520.
[63] M. Kaempgen, C. K. Chan, J. Ma, Y. Cui, G. Gruner, *Nano Lett.* **2009**, *9*, 1872.
[64] L. Yuan, X.-H. Lu, X. Xiao, T. Zhai, J. Dai, F. Zhang, B. Hu, X. Wang, L. Gong, J. Chen, C. Hu, Y. Tong, J. Zhou, Z. L. Wang, *ACS Nano* **2012**, *6*, 656.
[65] Y. J. Kang, H. Chung, C.-H. Han, W. Kim, *Nanotechnology* **2012**, *23*, 065401.
[66] H. H. Xu, X. L. Hu, H. L. Yang, Y. M. Sun, C. C. Hu, Y. H. Huang, *Adv. Energy Mater.* **2015**, *5*, 1401882.
[67] S. Chen, J. Zhu, X. Wu, Q. Han, X. Wang, *ACS Nano* **2010**, *4*, 2822.
[68] Y. J. Kang, S.-J. Chun, S.-S. Lee, B.-Y. Kim, J. H. Kim, H. Chung, S.-Y. Lee, W. Kim, *ACS Nano* **2012**, *6*, 6400.
[69] J. Sun, J. Wang, Z. Li, Z. Yang, S. Yang, *RSC Adv.* **2015**, *5*, 51773.
[70] X. Yang, C. Cheng, Y. Wang, L. Qiu, D. Li, *Science* **2013**, *341*, 534.